

CIRCUMSTELLAR MAGNETITE FROM THE LAP 031117 CO3.0 CHONDRITE

THOMAS J. ZEGA¹, PIERRE HAENECOUR^{2,3}, CHRISTINE FLOSS², AND RHONDA M. STROUD⁴¹ Lunar and Planetary Laboratory, University of Arizona, 1629 E. University Blvd, Tucson, AZ 85721-0092, USA; tzega@lpl.arizona.edu² Laboratory for Space Sciences and Physics Department, Washington University, One Brookings Drive, Campus Box 1105, St. Louis, MO 63130, USA³ Department of Earth and Planetary Sciences, Washington University, One Brookings Drive, Campus Box 1169, St. Louis, MO 63130, USA⁴ Materials Science and Technology Division, Code 6366, Naval Research Laboratory, 4555 Overlook Ave, SW Washington, DC 20375, USA

Received 2015 February 1; accepted 2015 June 7; published 2015 July 17

ABSTRACT

We report the first microstructural confirmation of circumstellar magnetite, identified in a petrographic thin section of the LaPaz Icefield 031117 CO3.0 chondrite. The O-isotopic composition of the grain indicates an origin in a low-mass ($\sim 2.2 M_{\odot}$), approximately solar metallicity red/asymptotic giant branch (RGB/AGB) star undergoing first dredge-up. The magnetite is a single crystal measuring 750×670 nm, is free of defects, and is stoichiometric Fe_3O_4 . We hypothesize that the magnetite formed via oxidation of previously condensed Fe dust within the circumstellar envelope of its progenitor star. Using an empirically derived rate constant for this reaction, we calculate that such oxidation could have occurred over timescales ranging from approximately ~ 9000 – $500,000$ years. This timescale is within the lifetime of estimates for dust condensation within RGB/AGB stars.

Key words: circumstellar matter – stars: AGB and post-AGB – stars: evolution – stars: formation – stars: fundamental parameters – stars: winds, outflows

INTRODUCTION

Refractory dust grains formed during the dying stages of ancient stars were injected into the local part of our galaxy where our solar system formed over 4.5 billion years ago. Such presolar circumstellar materials were incorporated into primitive meteorites, the physical relics leftover from our solar system's birth. Locked up within their crystal chemistry and structure are snapshots of the state of the stars when the circumstellar grains condensed. Probing these materials can provide ground-truth information on nucleosynthetic processes that occurred in their parent stars, the thermodynamics that took place in the circumstellar envelopes (CSE) from which they condensed, transport and irradiation processes within the interstellar medium, and secondary processes that could have affected them during solar system evolution (e.g., Zinner 2014).

Many types of circumstellar grains have been identified since their discovery over 25 years ago. These include: C-bearing materials such as graphitic C, SiC, and nanometer-sized grains of diamond (Bernatowicz et al. 1987; Lewis et al. 1987; Amari et al. 1990); silicates such as Mg, Fe-bearing glasses, pure silica, pyroxene and olivine; several types of oxides such as corundum, hibonite, spinel, Fe-, Mg-, Al-, and Ti-rich oxides (Nittler 1997; Nittler et al. 1997, 1998; Choi et al. 1999; Messenger et al. 2003, 2005; Zinner et al. 2003, 2005; Mostefaoui & Hoppe 2004; Nguyen & Zinner 2004; Vollmer et al. 2007, 2009, 2013; Floss et al. 2008; Floss & Stadermann 2009, 2012; Bose et al. 2010, 2012; Gyngard et al. 2010; Keller & Messenger 2011; Zega et al. 2011, 2014; Leitner et al. 2012; Haenecour et al. 2013b); and exotic materials such as Si_3N_4 (Alexander 1993; Nittler et al. 1995; Hoppe et al. 1996; Nittler 2003; Stroud et al. 2006). In general, the abundances of such materials vary according to the history of the meteorite in which they are found, i.e., whether the meteorite experienced secondary effects such as heating or aqueous-phase processing or whether it escaped such processing and remained relatively pristine since its accretion in the early solar system. Estimates place nanodiamonds as the most abundant (but least

understood) presolar-grain type, followed by silicates, SiC, spinel, graphite, corundum, Si_3N_4 , and other materials (Mostefaoui & Hoppe 2004; Nguyen et al. 2007; Floss & Stadermann 2009; Vollmer et al. 2009; Zinner 2014 and references therein).

Presolar oxide grains, while not as abundant as presolar silicates or SiC, are nonetheless important. Calculations predict oxide formation in the outflows of AGB stars and in the condensation sequence of our solar system (Yoneda & Grossman 1995; Gail & Sedylmayr 1999; Ebel & Grossman 2000; Lodders 2003). It has been suggested that oxide dust grains such as corundum and/or spinel may be responsible for the $13 \mu\text{m}$ emission feature of IR spectra of O-rich AGB stars (Onaka et al. 1989; Kozasa & Sogawa 1997; Posch et al. 1999; Speck et al. 2000), and comparison of remotely sensed infrared and laboratory-based spectra suggests that the oxide hibonite ($\text{CaAl}_{12}\text{O}_{19}$) may occur in planetary nebulae (Hofmeister et al. 2004).

Over 700 presolar oxide grains have thus far been identified (Presolar Grain Database, Hynes & Gyngard 2009) and elemental compositions are known for most of these. Such grains include aluminum oxide (Al_2O_3 , corundum in some cases) hibonite, Mg–Al and Fe–Cr-rich spinel, wüstite/magnesiowüstite (FeO), Ti-oxide, and TiO_2 , and have provided insight into nucleosynthetic processes for red/asymptotic giant branch (RGB/AGB) stars, supernovae, and galactic chemical evolution (Nittler 1997; Zinner et al. 2005; Floss et al. 2008; Bose et al. 2010, 2012; Nittler & Gaidos 2012; Zinner 2014). Crystal chemical and structural investigation of these materials unequivocally confirms their mineralogical identity and can provide complementary information on circumstellar thermodynamics, interstellar transport, and solar-system evolution. However, mineralogical analysis of presolar grains lags far behind the isotopic analyses due to the small sizes (nm to μm) of many of these grains and the complexity of extracting them from acid-resistant residues or petrographic thin sections for detailed microstructural analysis. Over the past decade, the number of grains for which coordinated isotopic and mineralogical data sets have been acquired has steadily increased due

to the viability of focused-ion-beam scanning-electron microscopy (FIB-SEM) as a tool for presolar grain research (Stroud et al. 2004; Nguyen et al. 2007; Vollmer et al. 2007, 2009; Zega et al. 2007; Bose et al. 2012; Leitner et al. 2012). Here we report on the first microstructural confirmation of circumstellar magnetite (Fe_3O_4). Our goal is to understand its detailed microstructure and what that can tell us about its origin in the CSE of its progenitor star.

Magnetite is a spinel-group mineral. Spinel has face-centered cubic structures (space group $\text{Fd}\bar{3}\text{m}$) and have a generalized formula of XY_2O_4 , where $\text{X} = \text{Mg}, \text{Fe}, \text{Ni}$, and $\text{Y} = \text{Fe}, \text{Al}, \text{Ti}$, and Cr . The lattice constant for spinel ranges from 0.808 to 0.854 nm and there are 32 O atoms and 24 cations in the unit cell. The cations are distributed among “A” and “B” positions with the former housing 8 cations in tetrahedral coordination and the latter containing 16 in octahedral coordination. The oxygen sublattice is arranged in cubic close packing parallel to the [111] direction, and layers of oxygen atoms alternate with layers of cations. Spinel can form two types of structures referred to as “normal” or “inverse” depending upon how the cations populate the A or B sites. A normal spinel contains 8 divalent cations in the A site and 16 trivalent cations in the B site (e.g., MgAl_2O_4). An inverse spinel contains 8 trivalent cations in the A site, with 8 divalent cations and 8 trivalent cations in the B site. Magnetite is an inverse spinel and can therefore be written as $\text{Fe}^{3+}(\text{Fe}^{2+}, \text{Fe}^{3+})\text{O}_4$, but is more commonly expressed as Fe_3O_4 (see Deer et al. 1992 for a discussion of spinel structure and crystal chemistry). Magnetite occurs in the matrices, chondrules, and fine-grained rims of primitive meteorites and exhibits a wide range of morphologies (Jedwab 1967; Kerridge 1970; Kerridge et al. 1979; Hyman et al. 1985; Brearley 1993; Buseck & Hua 1993; Choi et al. 1997; Krot et al. 1997; Hua & Buseck 1998). Though not a predicted condensate in the early solar nebula, it is hypothesized to form as an oxidation product of Fe metal (Yoneda & Grossman 1995; Hong & Fegley 1998; Ebel & Grossman 2000; Lodders 2003) and through aqueous-phase reactions on meteorite parent bodies (Kerridge 1970; Kerridge et al. 1979; Hyman et al. 1985; Krot et al. 1997; Hua & Buseck 1998).

SAMPLES AND METHODS

LaPaz Icefield 031117 (LAP 031117) is a type 3.0 CO chondrite that contains abundant presolar grains in its matrix and in fine-grained rims around chondrules (Haenecour & Floss 2012, 2013). A petrographic thin section of the meteorite, obtained from the curatorial facility at NASA Johnson Space Center, was examined with the Washington University NanoSIMS 50 to search for presolar grains. Carbon and O raster ion imaging was carried out on matrix-rich areas of the meteorite, following standard procedures (Floss & Stadermann 2009).

From among the O-rich presolar grains identified by Haenecour & Floss (2012, 2013), we selected grain LAP-103 measuring $\sim 550 \times 700$ nm, for detailed structural and chemical analysis with transmission electron microscopy (TEM). We used the Auger Nanoprobe at Washington University to acquire Auger elemental distribution maps of the grain. We then prepared an electron-transparent cross section of the grain using an FEI Nova 200 dual beam FIB-SEM located at Arizona State University. Our general approach is similar to methods that we have used previously for small (hundreds of nm) grains

(Stroud et al. 2004; Nguyen et al. 2007; Zega et al. 2007, 2011, 2014; Bose et al. 2010), i.e., deposition of protective Pt and/or C straps (to mitigate ion implantation and radiation damage during ion milling) on top of the hotspot, cross sectioning, extraction, and in situ thinning. However, given the fact that grain LAP-103 occurs in situ with other matrix grains in LAP 031117, we took extra measures to mark its position in order to assist us in preparation of the section as well as identification of the end point during in situ thinning. Thus, we used the electron beam to deposit a Pt strap on top of the area identified as the grain. The rectangular-shaped strap (approximately 515 nm wide \times 597 nm long) was oriented to transect the longest dimension of the grain, and extended to matrix material a few nm outside of the hotspot. After the initial strap of Pt was deposited, we used the Ga^+ ion beam to deposit a larger (12.5 μm long \times 1 μm wide \times 1.5 μm thick) strap of C on top of the initial markers. The use of the electron beam to deposit Pt provides an initial thin protective coating prior to exposing the area to the ion beam for final strap deposition and milling.

The FIB section was examined using a 200 keV JEOL 2200FS TEM at the Naval Research Laboratory (Washington, DC). The 2200FS is equipped with an energy-dispersive X-ray spectrometer (EDS) and bright-field (BF) and dark-field (DF) scanning TEM (STEM) detectors. The DF images were acquired using 80 and 175 mrad collection semi-angles, the contrast of which follows a $Z^{1.5}$ to Z^2 dependency that we have confirmed previously for this microscope (Zega et al. 2006). The grain composition was measured and quantified from a spectrum image acquired using a ThermoElectron Si(Li) EDS detector. The illumination conditions were adjusted to optimize counting statistics (high count rate, minimize beam damage, spectrometer dead time $\leq 30\%$) and included a 0.7 nm probe, 50 μs dwell time, and a total integration time of 10 minutes, which generated over 24,000 total counts. We used a standardless quantification of the spectrum image based on a Cliff-Lorimer thin-film matrix correction and Gaussian peak fits. The accuracy of the software k -factor for Fe was verified previously using San Carlos Olivine (Zega et al. 2011). The quality of the peak fitting was verified using simulated spectra and analysis of the residual intensity after subtraction using the SpectraCheck feature in Noran System Six software. The quality of the standardless quantification was based on reduced chi-squared values. Mineral stoichiometry was determined assuming the grain is an oxide with Fe in a mixed valence state as Fe_3O_4 and four O atoms per formula unit. The EDS detection limit is estimated at ≤ 0.1 wt% and the error is based on counting statistics.

Grain structure was determined using selected-area electron-diffraction (SAED) patterns. All SAED patterns were measured both manually (using Adobe Photoshop) and with the Crystallographic Image Processing Software Package (CRISP, Hovmöller 1992) based on calibrated camera constants. Indexing of the diffraction patterns was based on the cubic magnetite structure and lattice constant, and verified with simulated patterns that were calculated with the CrystalMaker software package.

RESULTS

NanoSIMS raster ion imaging (Figure 1) shows that grain LAP-103 is characterized by excess in ^{17}O relative to solar and a solar $^{18}\text{O}/^{16}\text{O}$ ratio ($^{17}\text{O}/^{16}\text{O} = (35.5 \pm 0.6) \times 10^{-4}$;

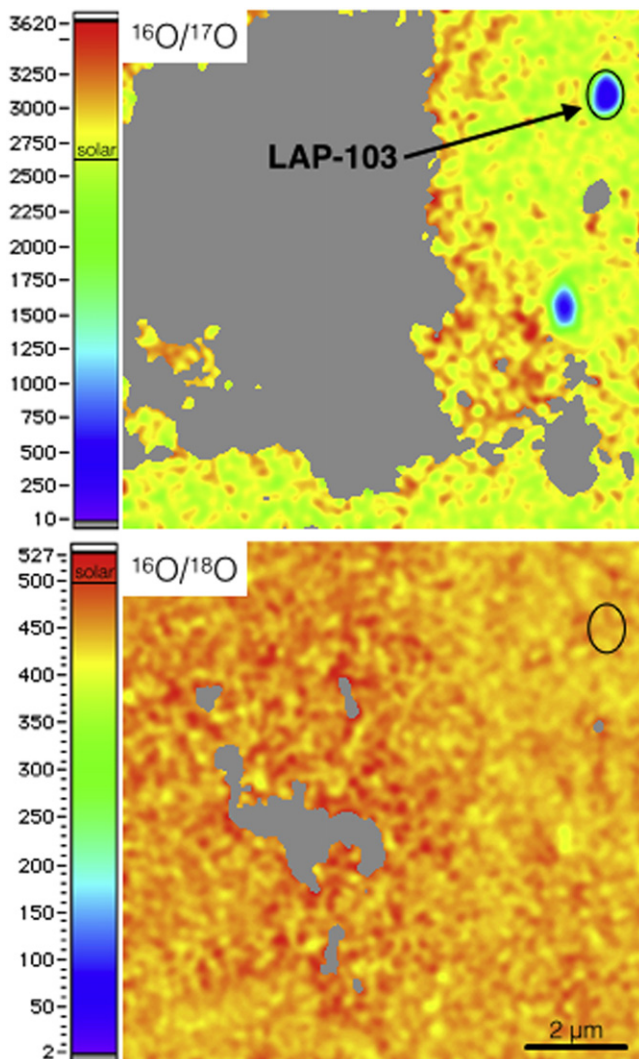


Figure 1. NanoSIMS $^{16}\text{O}/^{17}\text{O}$ and $^{16}\text{O}/^{18}\text{O}$ ratio images showing the oxygen isotopic composition of grain LAP-103.

$^{18}\text{O}/^{16}\text{O} = (2.05 \pm 0.04) \times 10^{-3}$; Haenecour et al. 2013a), which places it within the Group 1 field, as originally defined by Nittler (1997). Auger elemental distribution maps indicate that grain LAP-103 consists only of Fe and O (Figure 2).

Secondary electron images of the area containing LAP-103 reveal several coarse (μm) grains set within a porous fine-grained ($<1 \mu\text{m}$) matrix (Figure 3). Although the matrices of petrologic type-3 chondrites can be inherently porous, the porosity that occurs on the surface (Figure 3(a)) is likely a result of the ion-raster imaging from the SIMS analysis. Two isotopically anomalous regions (LAP-103 and LAP-104, the latter of which will be the subject of a future paper) occur within this local area of the sample, and we deposited Pt fiducial markers (see methods above) on them to locate and place the position of the protective carbon strap prior to ion milling (Figure 3(b)).

TEM imaging shows the localized area corresponding to O-isotopic anomaly LAP-103, just below the Pt cap deposited as a fiducial marker (see the methods section above) prior to ion-beam milling (Figure 4). The area beneath the Pt marker contains a triangular-shaped grain, with subhedral to anhedral morphology, measuring approximately $750 \text{ nm} \times 670 \text{ nm}$ in

orthogonal dimensions (Figure 4). SAED patterns acquired across LAP-103 show that it is a single crystal (Figure 5) and measurements of the patterns are consistent with and indexed to the magnetite spinel structure. X-ray spectrum imaging shows that the grain contains only Fe and O (Figure 6) and quantification gives stoichiometric Fe_3O_4 ($42.86 \pm 0.29 \text{ at\% Fe}$; 57.14 at\% O), corroborating the SAED data. LAP-103 is surrounded by coarse (μm -sized) grains and resides on top of a locally porous network composed mostly of nanocrystalline Mg silicates (Figure 6). The grain does not show any obvious sign of surface amorphization or alteration rims, and appears to be free of defects. The HAADF image shows localized contrast variations in the grain that EDS mapping confirms are due to the re-deposition of Pt during ion-beam milling (Figure 6).

DISCUSSION

The TEM data unambiguously identify LAP-103 as a single crystal of magnetite (cf., Figures 5 and 6). The majority of presolar oxide grains for which there are structural data are single crystals, however polycrystalline and amorphous grains have been reported. For example, Stroud et al. (2004) reported on two Al_2O_3 grains that condensed in the CSEs around AGB stars. TEM analysis showed that one grain is corundum, whereas the other is amorphous Al_2O_3 , and they concluded that AGB stars can condense corundum directly without more refractory (e.g., TiO_2) nucleation seeds. More recently, Takigawa et al. (2014a, 2014b) measured several presolar Al_2O_3 grains and reported that although most are single crystals some contain titanium oxide subgrains likely formed by exsolution. In comparison, Zega et al. (2011) reported on five presolar hibonite (nominally $\text{CaAl}_{12}\text{O}_{19}$) grains, four of which condensed in the circumstellar environments around RGB/AGB stars and one that condensed in the ejecta of a Type II supernova. SAED patterns of all five grains show that they are single crystals with minor orientation spreads across the grains and little to no defects. The single-crystal nature and stoichiometric compositions of these hibonite grains were inferred to be generally consistent with theoretical predictions for condensation, suggesting condensation temperatures between 1480 and 1743 K, assuming total gas pressures between 1×10^{-6} and 1×10^{-3} atm. In a separate study, Zega et al. (2014) reported on the microstructural properties of four presolar spinel grains whose isotopic compositions indicate origins in low-mass O-rich AGB stars. Three of the grains are single crystal Mg–Al-rich spinels containing minor Fe and Cr, whereas the fourth spinel consists of a polycrystalline assemblage of three Fe–Cr rich grains with closely aligned crystallographic orientation but systematically varied cation composition. As with the hibonite grains discussed above, the properties of single-crystal, stoichiometric, nearly pure Mg–Al spinels were inferred to be generally consistent with equilibrium condensation predictions, suggesting condensation temperatures between 1161 and 1221 K, assuming total gas pressures between 1×10^{-6} and 1×10^{-3} atm, whereas the Fe–Cr-rich spinels are inconsistent with such predictions and suggest a complex cooling history. The microstructural data sets for presolar oxide grains, although limited, seem to suggest that condensation of single-crystal stoichiometric grains is common in the CSEs of RGB/AGB stars. Similar studies on silicate stardust show more diversity, including amorphous and/or polycrystalline assemblages of widely varying composition, in addition to stoichiometric single crystals (e.g., Messenger et al.

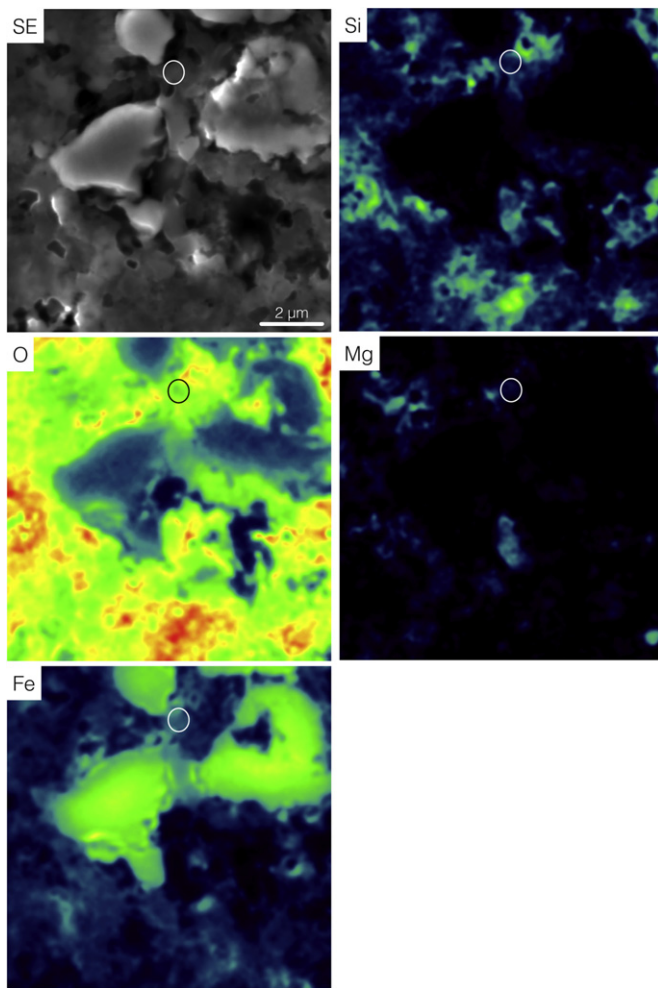


Figure 2. Secondary electron image (SE) and Auger elemental distribution maps of grain LAP-103.

2005; Vollmer et al. 2007, 2009; Busemann et al. 2009; Nguyen et al. 2010). The LAP-103 magnetite grain reported herein seems to be generally consistent with the trend so far observed for presolar oxides, i.e., it is a stoichiometric single crystal. However, the origin of magnetite, so far as we understand it from the meteoritic record, is somewhat controversial.

Magnetite has been previously identified in CO3.0 chondrites such as ALHA77307 (Brearley 1993) and other chondritic meteorites that span petrologic types 1 through 3 (Jedwab 1967; Kerridge 1970; Kerridge et al. 1979; Nagahara 1984; Hyman et al. 1985). It exhibits a range of morphologies including plaquettes, framboids, stacked platelets, spherules, and trapezohedral grains (e.g., Kerridge 1970; Hyman et al. 1985; Hua & Buseck 1998). Such morphologies likely reflect different formation histories, which are proposed to include condensation in the solar nebula (Nagahara 1984; Brearley 1993), gas-solid reaction of pre-existing material (e.g., Fe metal or perovskite) in the solar nebula (Kerridge 1970; Kurat et al. 2002), and aqueous-phase reactions on the asteroid parent bodies of meteorites (Kerridge et al. 1979; Choi et al. 1997; Krot et al. 1997; Hua & Buseck 1998; Bullock et al. 2005). Our TEM work (Haenecour et al. 2014, 2015) shows that the matrix of LAP 031117 did experience limited and localized alteration. However, we find no evidence of

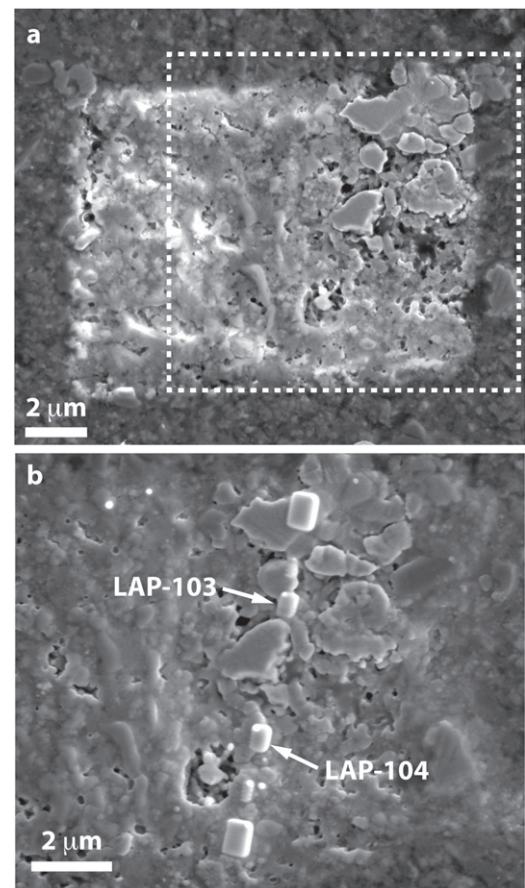


Figure 3. Plan-view secondary electron images of the matrix of the LAP 031117 CO3.0 chondrite. (a) Area 7C-8 after SIMS analysis but prior to FIB-SEM extraction. (b) Local region of interest indicated by the white-dashed box in (a). The image was acquired after deposition of Pt fiducial markers on top of the isotopic hotspots containing LAP-103 and LAP-104, but prior to deposition of the protective C strap.

hydration in this FIB section, such as the presence of sheet silicates or carbonates, which might otherwise suggest the possibility that secondary alteration on the parent body could have led to the formation of grain LAP-103. We infer, therefore, from the homogeneous composition and the lack of evidence for secondary alteration that the magnetite retained the structural and chemical properties it acquired during condensation in the CSE of its progenitor star. To our knowledge, this is the first definitive microstructural identification of presolar magnetite. Croat et al. (2008) identified a possible magnetite subgrain (~ 30 nm) within a presolar graphite ultramicrotome sections, but its small size precluded isotopic analysis and, thus, verification of its presolar origin.

The isotopic compositions of presolar grains reflect the nucleosynthetic processes that occurred in their parent stars. Relative to other presolar oxide grains, LAP-103 plots within the Group-1 field as originally defined by Nittler (1997). The O-isotopic trend of the Group 1 grains can be reproduced by nucleosynthetic models of low-mass (1 to ~ 2 – $2.5 M_{\odot}$) stars on the red giant or asymptotic giant-branch stage of stellar evolution undergoing first dredge-up episodes (Boothroyd et al. 1994; Huss et al. 1994; Wasserburg et al. 1995; Nittler 1997; Nittler et al. 2008; Boothroyd & Sackmann 1999). As the $^{17}\text{O}/^{16}\text{O}$ ratio depends on the mass of the star and the $^{18}\text{O}/^{16}\text{O}$ ratio depends on its metallicity, the O isotopic

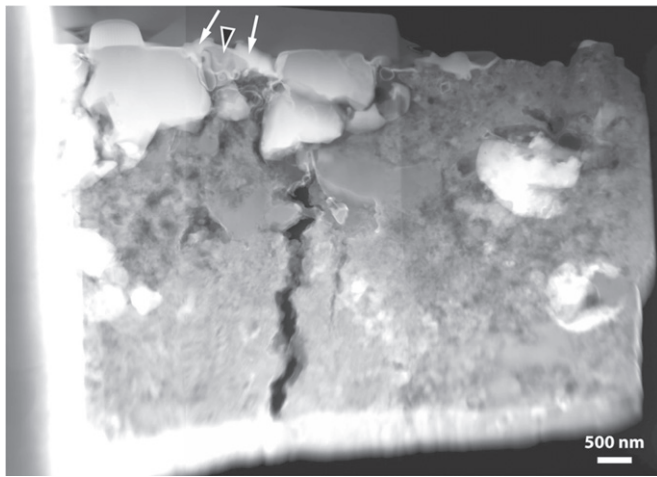
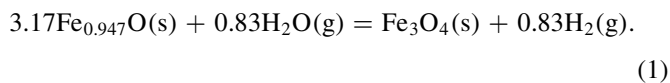


Figure 4. High-angle annular-dark-field image of the FIB section extracted from LAP 031117 along the line transecting the LAP-103 and LAP-104 hotspots (cf, Figure 1(b)). Grain LAP-103 (indicated by the black arrowhead with white outline) occurs beneath the Pt fiducial marker (indicated by the white arrows).

composition of a presolar grain can also be used to estimate the progenitor star’s mass and initial metallicity. The O isotopic composition of LAP-103 suggests that it condensed from an RGB star undergoing first dredge-up whose initial mass was approximately $1.8\text{--}2.2 M_{\odot}$ with a close to solar metallicity.

Knowledge of the progenitor star’s fundamental parameters can help place estimates on the conditions under which the magnetite could have formed. That the magnetite condensed in a close to solar-metallicity star and that we do not find any defects or non-stoichiometry in it, which would otherwise suggest that non-equilibrium played a role in its formation, we assume that equilibrium calculations, which model a condensing gas of solar composition, should be applicable. However, such calculations do not predict that magnetite will condense from the gas phase under canonical nebular conditions (Yoneda & Grossman 1995; Ebel & Grossman 2000; Lodders 2003; Ebel 2006), as Fe in the gas phase prefers to condense into metal. However, Palme & Fegley (1990) performed calculations that suggest that if the oxygen partial pressure were increased by several orders of magnitude above canonical values, then Fe_3O_4 could possibly condense in the early solar nebula. Although there may have been localized environments in the early solar nebula that could have provided such enhanced oxygen partial pressures, such conditions are not typically expected for the envelope around an AGB/RGB star of solar metallicity.

An alternative pathway for magnetite formation is the oxidation of pre-existing oxide or metal grains. Wüstite ($\text{Fe}_{0.947}\text{O}$) can be oxidized to form magnetite via:



However, oxidation of wüstite to form magnetite is not expected under canonical water-to-hydrogen ratios (5.53×10^{-4} to 1.26×10^{-3} ; see Hong & Fegley 1998), and hence oxygen fugacities, expected for a solar composition gas.

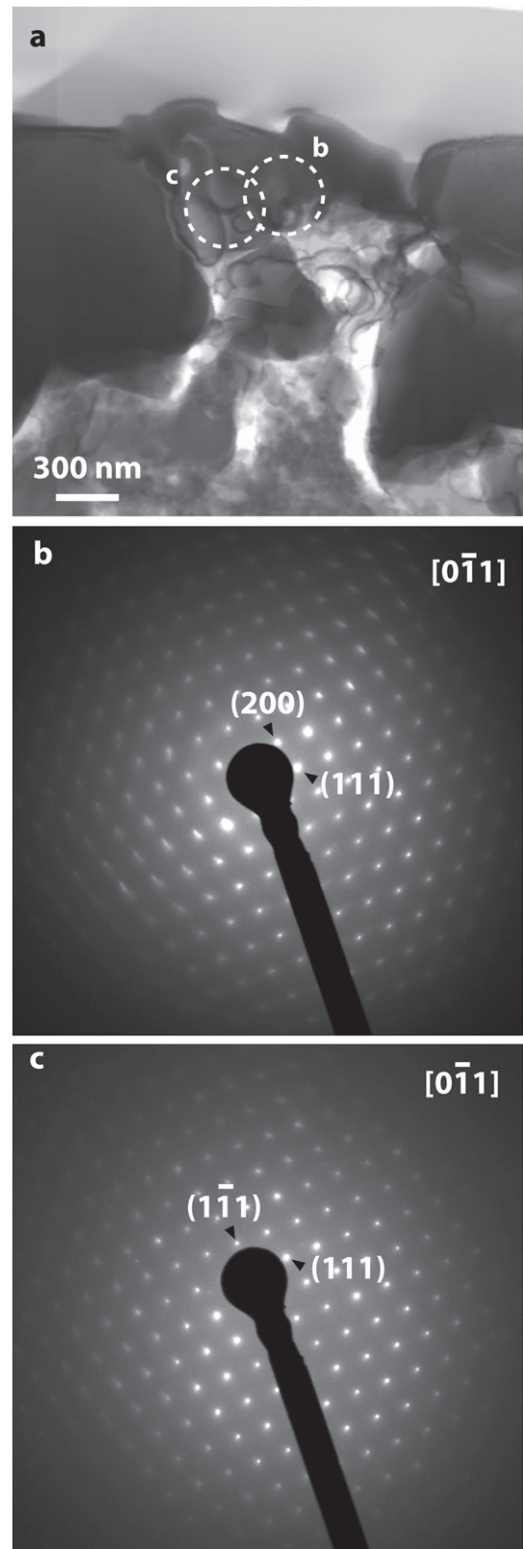


Figure 5. TEM data from grain LAP-103. (a) Bright-field scanning TEM (STEM) image showing local grain. (b), (c) SAED patterns acquired from the grain in the areas indicated by the white-dashed circles in (a). Both patterns were acquired with the sample oriented at the same tilt angle ($t_x = -16^\circ 3'$, $t_y = -1^\circ 2'$) and both index to the same zone axis $[0\bar{1}1]$ for magnetite. The black feature extending from the lower-right part of the image is the beam stop used to prevent over exposure of the CCD camera by the forward-scattered beam.

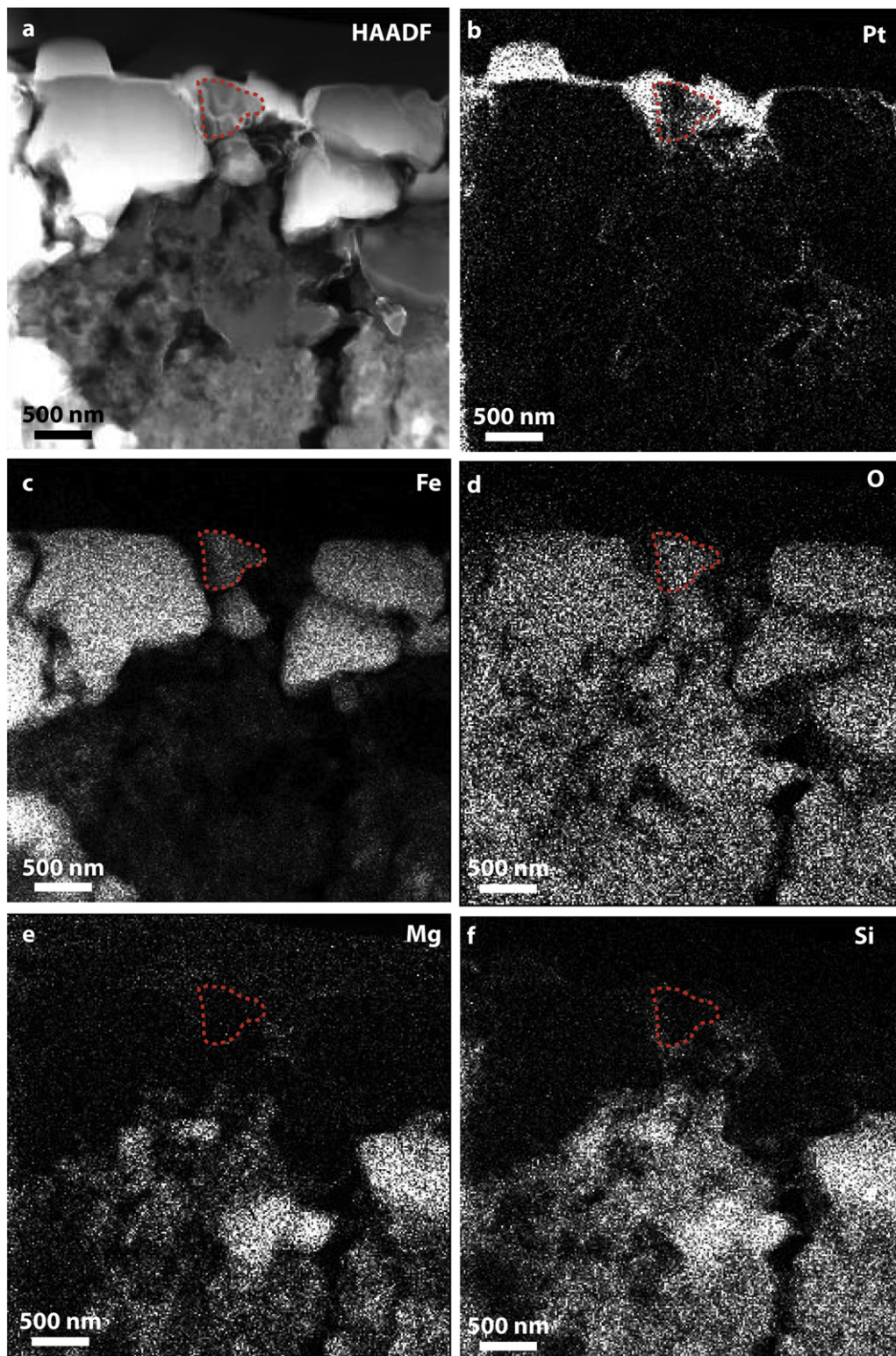


Figure 6. STEM data and spectrum-image maps on LAP-103 and the area of the FIB section local to it. (a) HAADF-STEM image. (b)–(f) X-ray maps of elements as indicated. The red-dashed line traces the outline of the grain. The maps were produced via $K\alpha$ X-ray emissions from all elements except Pt, for which the $M\alpha$ emission was used to avoid overlap from spurious $Cu K\beta$ X-rays emitted by the TEM support grid. The HAADF image shows the high-Z Pt fiducial marker, and the Pt map confirms its location and hence that of LAP-103.

Given that the O-isotopic composition of LAP-103 indicates that it formed in a CSE surrounding a close to solar-metallicity star and that the TEM data are consistent with a grain formed via equilibrium condensation, we rule out Reaction (1) as the

pathway of formation. Instead, we consider magnetite is formed through reaction of previously condensed Fe metal with O in the gas via:



Reaction (2) is independent of total pressure and only depends on the $\text{H}_2\text{O}/\text{H}_2$ ratio to control the O partial pressure. Hong & Fegley (1998) studied Reaction (2) experimentally at $\text{H}_2\text{O}/\text{H}_2$ ratios ranging from 2.44×10^{-2} to 2.44×10^{-1} , which are water-rich conditions relative to the estimated solar $\text{H}_2\text{O}/\text{H}_2$ ratio (noted above). They showed that magnetite formation should occur between 357 and 384 K, depending upon the availability of O to form water vapor, which, in turn, depends upon the distribution of C between CO and CH_4 in the gas phase. We note that water vapor has been detected in the CSEs surrounding C-rich AGB stars with $\text{H}_2\text{O}/\text{H}_2$ ratios as high as 9 (Melnick 2001) and M-type AGB stars may have $\text{H}_2\text{O}/\text{H}_2$ ratios of greater than 1 (Cherchneff 2006; Maercker et al. 2008; Decin et al. 2010). Given that the O-isotopic composition of LAP-103 indicates formation in the envelope of a close to solar-metallicity star, in which O and H are abundant, water vapor could have been a plausible oxidant of previously condensed Fe metal. We suggest that Reaction (2) was, therefore, the likely pathway by which the magnetite in LAP-103 formed and that it probably did so within a temperature range of approximately 350–400 K.

We can place constraints on the time it would take for Fe metal grains to completely oxidize to magnetite using the rate constants determined by Hong & Fegley (1998) for Reaction (2). We use their Equation (18) for the t_{100} lifetime (timescale for complete oxidation) and assume that grain LAP-103 was initially spherical with a maximum diameter of 700 nm based on the average grain size as measured from our BF-STEM and HAADF images (Figures 4 and 5). Using the rate constant determined for Reaction (2) from pure Fe powder, we calculate that complete oxidation could have required timescales ranging from approximately 9000–500,000 years for temperatures ranging from 400 to 350 K, respectively (Table 1). If we use the rate constant for Reaction (2) determined from metal filings of the Gibeon iron meteorite, the timescale for complete oxidation increases to approximately 325,000–19 Myr over the same temperature interval (Table 1). The rate constant for oxidation based on the metal filings of the Gibeon iron meteorite is significantly lower than that based on the pure Fe powder (leading to a shorter timescale for oxidation), which Hong & Fegley (1998) hypothesized was due to the former’s content of minor elements, most notably Ni, Co, and P. We do not detect minor elements in grain LAP-103, at least down to the ~ 0.1 at% detection limit of the Si(Li) EDS detector on the 2200FS TEM, and so infer that the rate constants determined from the pure Fe powder provide the more accurate constraint for the timescale of oxidation of grain LAP-103. Hong & Fegley (1998) noted that the calculated lifetimes for Fe alloy oxidation in the solar nebula might be considered lower limits because they were performed in relatively water-rich conditions. Thus, the magnetite formation rate would decrease under canonical nebular conditions with lower $\text{H}_2\text{O}/\text{H}_2$ ratios. In the case of LAP-103, its O isotopic composition suggests that it formed in a close to solar metallicity star, and so by analogy, the calculated lifetimes for Fe oxidation in its host CSE might also be regarded as lower limits. However, we note that the estimate of metallicity is model dependent. If the progenitor star of LAP-103 had a metallicity greater than solar, which could be suggested by the Boothroyd et al. (1994) model, we might expect the $\text{H}_2\text{O}/\text{H}_2$ ratio of its envelope to be higher because it will contain more abundant O. Thus, rates for

Table 1

Time (in years) for the Oxidation of an Fe Metal Grain Measuring 700 nm in Diameter Based on Rate Constants Derived from Pure Fe Powder (PFe) and Filings of the Gibeon Meteorite by Hong & Fegley (1998)

T (K)	PFe (years)	Gibeon (years)
400	8.9×10^3	3.3×10^5
375	5.7×10^4	2.2×10^6
350	4.7×10^5	1.9×10^7

Reaction (2) could have been higher than if the CSE of LAP-103 contained solar abundances of H and O. As we note above, water vapor has been detected in the CSEs of AGB stars with $\text{H}_2\text{O}/\text{H}_2$ ratios as high as 9 (Melnick 2001), and so it is conceivable that oxidation of an Fe alloy could proceed more rapidly than calculated (Table 1) under such conditions assuming sufficiently high pressures and collision rates of H_2O molecules and the metal surface. Nevertheless, to our knowledge, this is the first estimate of the kinetics of grain formation in the CSE of an RGB/AGB star from experimental data, and so it is reasonable to consider how the calculated grain-formation time compares with estimates for grain formation times in the CSEs of RGB/AGB stars.

AGB stars are the major dust producers in the galaxy, and so their dust-producing dynamics tend to be better investigated than those of RGB stars. For example, Ferrarotti & Gail (2006) modeled the composition and quantities of dust produced in the outflows of AGB stars. Their calculations show that the condensation of iron dust, through several thermal pulses, can span hundreds of thousands of years for stars with masses ranging from $1.0 M_\odot$ to $2.0 M_\odot$ and solar metallicity. Given the reaction pathway for magnetite formation and the reaction time we calculate for LAP-103, it is worth exploring whether a metal dust grain could reside within the CSE for that length of time reacting with available O to convert to it to an oxide.

Such a consideration requires knowledge of the rate at which the grain is moving, the trajectory of its transport, and the size of the CSE. The terminal wind velocity of most (86%) O-rich circumstellar envelopes ranges from 5 to 20 km s^{-1} (Loup et al. 1993; Sedylmayr & Dominik 1995) and the gas-loss rates are proportional to the dust-loss rates over the entire range of mass-loss (Knapp & Morris 1985; Sopka et al. 1985; Jura 1986; Sedylmayr & Dominik 1995). The trajectory of grain transport is impossible to know, but we can make a simplifying assumption that it either travels normal to the surface from which it is ejected, carried along by dust-driven wind, or through some random pathway within the CSE. Using the terminal wind velocities of 5 and 20 km s^{-1} and the calculated reaction time for grain LAP-103, we estimate that such a grain could have potentially traveled between 1.40×10^{12} and $3.0 \times 10^{14} \text{ km}$. Assuming that such transport occurred normal to the surface of the star and was uninterrupted, would such distances be within the range of the CSE in which oxidizing reactions could occur?

The size of the envelope will depend on the size of the star, its mass-loss, and its evolutionary state. For stars undergoing dredge-up episodes on the giant branch of stellar evolution, we expect that extensive envelopes will surround them. For example, the outer region of the spherically symmetric CSE of the O-rich AGB star IK Tauri is estimated to extend out to 20,000 stellar radii where it begins to intersect with the interstellar radiation field, a distance that is equivalent to

4×10^{14} km (Decin et al. 2010). This radial distance is outside of the 3.0×10^{14} km distance we estimate as an upper limit for LAP-103 if it were traveling normal to the surface from which it was ejected. As we note above, H_2O has been detected in the CSE of AGB stars (Melnick 2001; Cherchneff 2006; Maercker et al. 2008; Decin et al. 2010), and it (and other molecular species), are expected in the outer envelope, but its abundance (and temperature) is predicted to decrease significantly with increasing radial distance (Willacy & Millar 1997; Decin et al. 2010). Low temperature and partial pressure of oxygen would only increase the timescale for oxidation. Nonetheless, it is conceivable that such a grain traveling at velocities of $5\text{--}20 \text{ km s}^{-1}$ over timescales ranging from thousands to several hundred thousand years normal to the surface of the star, could remain and oxidize within the CSE of a giant star. On the other hand, it seems unlikely that a grain would travel uninterrupted along some initial trajectory normal to the CSE. It is more likely that the path of grain LAP-103 was much more complex and could have spent considerable time in the inner or intermediate CSE where H_2O would have been more abundant and provided the O needed to fully oxidize the Fe within the assemblage.

CONCLUSIONS

We report the first experimental confirmation of circumstellar magnetite identified within the matrix of the LAP 031117 CO3 chondrite. The O-isotopic data suggest the grain originated in a close to solar metallicity star with a mass approximately $2.2 M_{\odot}$ that evolved along the RGB/AGB branch of stellar evolution. TEM data reveal that the magnetite consists of a single, stoichiometric Fe_3O_4 crystal. We infer that the ~ 700 nm diameter grain formed at low temperature (350–400 K) in the CSE of its progenitor star. The TEM data are consistent with an origin through oxidation of previously condensed Fe metal. This reaction has been studied experimentally (Hong & Fegley 1998), and we use those results to place constraints on the kinetics of the proposed oxidation reaction within the circumstellar environment. Our calculations suggest that complete oxidation of previously condensed Fe metal dust to form the magnetite assemblage could have required timescales ranging from approximately 9000–500,000 years. Such timescales are within the lifetime of dust condensation for RGB/AGB stars undergoing dredge-up episodes.

We thank an anonymous reviewer for constructive comments that helped improve the manuscript. This research was supported by the NASA Cosmochemistry Program (grants NNX12AK47G to T.J.Z., NNX14AG25G to C.F., and NNX13AV45I to R.M.S.) and NASA Earth and Space Science Fellowship program (NNX12AN77H to P.H.).

REFERENCES

- Alexander, C. M. O'D. 1993, *GeCoA*, 57, 2869
 Amari, S., Anders, E., Virag, A., & Zinner, E. K. 1990, *Natur*, 345, 238
 Bernatowicz, T. J., Fraundor, G., Tang, M., et al. 1987, *Natur*, 330, 728
 Boothroyd, A. I., & Sackmann, I.-J. 1999, *ApJ*, 510, 232
 Boothroyd, A. I., Sackmann, I.-J., & Wasserburg, G. J. 1994, *ApJL*, 430, L77
 Bose, M., Floss, C., & Stadermann, F. 2010, *ApJ*, 714, 1624
 Bose, M., Floss, C., Stadermann, F., Stroud, R. M., & Speck, A. K. 2012, *GeCoA*, 93, 77
 Brearley, A. J. 1993, *GeCoA*, 57, 1521
 Bullock, E. S., Gounelle, M., Lauretta, D. S., Grady, M. M., & Russell, S. S. 2005, *GeCoA*, 69, 2687
 Buseck, P. R., & Hua, X. 1993, *AREPS*, 21, 255
 Busemann, H., Nguyen, A. N., Cody, G. D., et al. 2009, *E&PSL*, 288, 44
 Cherchneff, I. 2006, *A&A*, 456, 1001
 Choi, B. G., McKeegan, K. D., Leshin, L. A., & Wasson, J. T. 1997, *E&PSL*, 146, 337
 Choi, B. G., Wasserburg, G. J., & Huss, G. R. 1999, *ApJL*, 522, L133
 Croat, T. K., Stadermann, F., & Bernatowicz, T. 2008, *M&PS*, 43, 1497
 Decin, L., De Beck, E., Brünken, S., et al. 2010, *A&A*, 516, A69
 Deer, W. A., Howie, R. A., & Zussman, J. 1992, *An Introduction to the Rock-Forming Minerals* (Essex, UK: Longman Group, Ltd.)
 Ebel, D. S. 2006, in *Meteorites and the Early Solar System II*, ed. D. S. Lauretta, Jr. & H. Y. McSween (Tucson, AZ: Univ. Arizona Press), 253
 Ebel, D. S., & Grossman, L. 2000, *GeCoA*, 64, 339
 Ferrarotti, A. S., & Gail, H.-P. 2006, *A&A*, 447, 553
 Floss, C., & Stadermann, F. 2009, *GeCoA*, 73, 2415
 Floss, C., & Stadermann, F. 2012, *M&PS*, 47, 992
 Floss, C., Stadermann, F. J., & Bose, M. 2008, *ApJ*, 672, 1266
 Gail, H.-P., & Sedylmayr, E. 1999, *A&A*, 347, 594
 Gyngard, F., Zinner, E., Nittler, L. R., et al. 2010, *ApJ*, 717, 107
 Haenecour, P., & Floss, C. 2012, *LPI*, 43, 1107
 Haenecour, P., & Floss, C. 2013, *LPI*, 44, 1024
 Haenecour, P., Floss, C., Jolliff, B. L., & Carpenter, P. 2013a, *LPI*, 44, 1150
 Haenecour, P., Floss, C., Jolliff, B. L., et al. 2014, *LPI*, 45, 1316
 Haenecour, P., Zega, T. J., Floss, C., Croat, T. K., & Jolliff, B. L. 2015, *LPI*, 46, 1160
 Haenecour, P., Zhao, X., Floss, C., Lin, Y., & Zinner, E. K. 2013b, *ApJL*, 768, 1
 Hofmeister, A. M., Wopenka, B., & Locock, A. J. 2004, *GeCoA*, 68, 4485
 Hong, Y., & Fegley, B. J. 1998, *M&PS*, 33, 1101
 Hoppe, P., Strebel, R., Eberhardt, P., Amari, S., & Lewis, R. S. 1996, *GeCoA*, 60, 883
 Hovmöller, S. 1992, *Ultmi*, 41, 121
 Hua, X., & Buseck, P. R. 1998, *M&PS*, 33, A215
 Huss, G. R., Fahey, A. J., Gallino, R., & Wasserburg, G. J. 1994, *ApJL*, 430, L81
 Hyman, M., Ledger, E. B., & Rowe, M. W. 1985, *JGR*, 90, c710
 Hynes, K. M., & Gyngard, F. 2009, *LPI*, 40, 1198
 Jedwab, J. 1967, *E&PSL*, 2, 440
 Jura, M. 1986, *ApJ*, 303, 327
 Keller, L. P., & Messenger, S. 2011, *GeCoA*, 75, 5336
 Kerridge, J. F. 1970, *E&PSL*, 9, 299
 Kerridge, J. F., Mackay, A. L., & Boynton, W. V. 1979, *Sci*, 205, 395
 Knapp, G. R., & Morris, M. 1985, *ApJ*, 292, 640
 Kozasa, T., & Sogawa, H. 1997, *Ap&SS*, 251, 165
 Krot, A. N., Zolensky, M. E., Wasson, J. T., et al. 1997, *GeCoA*, 61, 219
 Kurat, G., Zinner, E., & Brandstatter, F. 2002, *GeCoA*, 66, 2959
 Leitner, J., Vollmer, C., Hoppe, P., & Zipfel, J. 2012, *ApJ*, 745, 38
 Lewis, R. S., Tang, M., Wacker, J. F., Anders, E., & Steel, E. 1987, *Natur*, 326, 160
 Lodders, K. 2003, *ApJ*, 591, 1220
 Loup, C., Forveille, T., Omont, A., & Paul, J. F. 1993, *A&AS*, 99, 291
 Maercker, M., Schöier, F. L., Olofsson, H., Bergman, P., & Ramstedt, S. 2008, *A&A*, 479, 779
 Melnick, G. J. 2001, *Natur*, 412, 160
 Messenger, S., Keller, L. P., & Lauretta, D. S. 2005, *Sci*, 309, 737
 Messenger, S., Keller, L. P., Stadermann, F. J., Walker, R. M., & Zinner, E. 2003, *Sci*, 300, 105
 Mostefaoui, S., & Hoppe, P. 2004, *ApJL*, 613, L149
 Nagahara, H. 1984, *GeCoA*, 48, 2581
 Nguyen, A., Nittler, L. R., Stadermann, F. J., Stroud, R. M., & Alexander, C. M. O'D. 2010, *ApJ*, 719, 166
 Nguyen, A. N., Stadermann, F. J., Zinner, E., et al. 2007, *ApJ*, 656, 1223
 Nguyen, A. N., & Zinner, E. 2004, *Sci*, 303, 1496
 Nittler, L., Alexander, C. M. O'D., Gao, X., Walker, R. M., & Zinner, E. 1997, *ApJ*, 483, 475
 Nittler, L. R. 1997, in *Astrophysical Implications of the Laboratory Study of Presolar Materials*, ed. T. Bernatowicz & E. Zinner (New York: AIP), 59
 Nittler, L. R. 2003, *E&PSL*, 209, 259
 Nittler, L. R., Alexander, C. M. O'D., Gallino, R., et al. 2008, *ApJ*, 682, 1450
 Nittler, L. R., Alexander, C. M. O'D., Wang, J., & Gao, X. 1998, *Natur*, 393, 222
 Nittler, L. R., & Gaidos, E. 2012, *M&PS*, 47, 2031
 Nittler, L. R., Hoppe, P., Alexander, C. M. O'D., et al. 1995, *ApJL*, 453, L25

- Onaka, T., Jong, T. D., & Willems, F. J. 1989, *A&A*, **218**, 169
- Palme, H., & Fegley, B. J. 1990, *E&PSL*, **101**, 180
- Posch, T., Kerschbaum, F., Mutschke, H., et al. 1999, *A&A*, **352**, 609
- Sedylmayr, E., & Dominik, C. 1995, *SSRv*, **73**, 211
- Sopka, R. J., Hildebrand, R., Jaffe, D. T., et al. 1985, *ApJ*, **294**, 242
- Speck, A. K., Barlow, M. J., Sylvester, R. J., & Hofmeister, A. M. 2000, *A&AS*, **146**, 437
- Stroud, R. M., Nittler, L. R., & Alexander, C. M. O'D. 2004, *Sci*, **305**, 1455
- Stroud, R. M., Nittler, L. R., & Alexander, C. M. O'D. 2006, *M&PS*, **41** (Supp.), Abstract# 5360
- Takigawa, A., Stroud, R. M., Nittler, L. R., & Alexander, C. M. O'D. 2014a, *M&PS*, **49**, A390
- Takigawa, A., Stroud, R. M., Nittler, L. R., et al. 2014b, *LPI*, **45**, 1465
- Vollmer, C., Brenker, F. E., Hoppe, P., & Stroud, R. M. 2009, *ApJ*, **700**, 774
- Vollmer, C., Hoppe, P., & Brenker, F. E. 2013, *ApJ*, **769**, 61
- Vollmer, C., Hoppe, P., Brenker, F. E., & Holzapfel, C. 2007, *ApJL*, **666**, L49
- Wasserburg, G. J., Boothroyd, A. I., & Sackmann, I.-J. 1995, *ApJL*, **447**, L37
- Willacy, K., & Millar, T. J. 1997, *A&A*, **324**, 237
- Yoneda, S., & Grossman, L. 1995, *GeCoA*, **59**, 3413
- Zega, T. J., Alexander, C. M. O'D., Nittler, L. R., & Stroud, R. M. 2011, *ApJ*, **730**, 83
- Zega, T. J., Hanbicki, A. T., Erwin, S. C., et al. 2006, *PhRvL*, **96**, 196101
- Zega, T. J., Nittler, L. R., Busemann, H., Hoppe, P., & Stroud, R. M. 2007, *M&PS*, **42**, 1373
- Zega, T. J., Nittler, L. R., Gyngard, F., et al. 2014, *GeCoA*, **124**, 152
- Zinner, E., Amari, S., Guinness, R., et al. 2003, *GeCoA*, **67**, 5083
- Zinner, E., Nittler, L. R., Hoppe, P., et al. 2005, *GeCoA*, **69**, 4149
- Zinner, E. K. 2014, in *Meteorites, Comets, and Planets*, ed. A. M. Davis (New York: Elsevier), 181